Signal Processing 150 (2018) 51–56

Contents lists available at ScienceDirect

Signal Processing

journal homepage: www.elsevier.com/locate/sigpro

Short communication

Mixed far-field and near-field source localization based on subarray cross-cumulant[☆]

Zhi Zheng[a,*], Mingcheng Fu[a], Wen-Qin Wang[a], Hing Cheung So[b]

[a] School of Information and Communication Engineering, University of Electronic Science and Technology of China, Chengdu 611731, China
[b] Department of Electronic Engineering, City University of Hong Kong, Hong Kong, China

ARTICLE INFO

Article history:
Received 9 January 2018
Revised 27 March 2018
Accepted 28 March 2018
Available online 29 March 2018

Keywords:
Far-field
Near-field
Source localization
Uniform linear array (ULA)
Cross-cumulant

ABSTRACT

This paper presents a new algorithm for mixed far-field and near-field source localization using a uniform linear array (ULA). Firstly, the ULA is divided into two overlapping subarrays to construct two special cross-cumulant matrices of the subarray outputs, which are only characterized by directions-of-arrival (DOAs) of the sources. Then, the shift invariance structure in the cumulant domain is derived, and the DOAs of all sources are estimated by the TLS-ESPRIT method. Finally, with the estimated DOAs, the range estimates of near-field sources are obtained via one-dimensional search, and the types of sources are also distinguished. The developed algorithm involves neither DOA search nor parameter pairing. Furthermore, it exhibits a higher localization accuracy than the traditional methods. Simulation results are presented to demonstrate the performance of the proposed algorithm.

© 2018 Elsevier B.V. All rights reserved.

1. Introduction

Source localization is a fundamental problem in many fields such as radar, sonar, wireless communications, electronic surveillance and seismic exploration [1–4]. In the past decades, lots of high-resolution methods like MUSIC [5] and ESPRIT [6] have been developed to locate far-field (FF) sources, i.e., direction-of-arrival (DOA) estimation. In near-field (NF) source scenarios, both DOA and range parameters need to be estimated, and various algorithms [7–20] were also presented for near-field source localization.

However, in some practical applications, both FF and NF sources may coexist. In the mixed source scenarios, the pure FF or NF localization methods may be invalid. To tackle this issue, some new approaches have been recently developed, including high-order MUSIC [21], second-order MUSIC [22], mixed-order MUSIC [23], sparse reconstruction methods [24,25], spatial differencing methods [26,27] and others [28–30]. The aforementioned approaches [21–25,29] estimate the DOAs of sources using MUSIC spectrums or sparse recovery techniques. Therefore, they are computationally intensive. Although other methods [26–28,30] implement DOA estimation by the generalized ESPRIT method[31] based on two shift subarrys, the generalized ESPRIT method [31] still need to perform spectral search different from the traditional ESPRIT method [6]. The high-order ESPRIT method [11] can achieve search-free DOA estimates, but it is limited to the near-field source scenarios. Moreover, the high-order ESPRIT method [11] only exploits half of the array degree of freedom and involves parameter pairing processing.

To overcome the above drawbacks, in this paper, we devise a new algorithm for mixed source localization using a uniform linear array (ULA). Firstly, we design two special cross-cumulant matrices based on two overlapping subarrays of the ULA, and derive the shift invariance structure in the cumulant domain. Then, the DOAs of all sources are estimated by the total least squares (TLS)-ESPRIT method. Finally, with the DOA estimates, the ranges of near-field sources are estimated by one-dimensional (1-D) search and the types of sources are also distinguished. Our approach avoids DOA search and parameter pairing process, and it provides an improved localization accuracy. Its superiorities over the traditional methods are verified by simulation results.

Notation: The superscripts $*$, T, H and $\dagger$ denote the conjugate, transpose, conjugate transpose and pseudo-inverse, respectively; $E\{\cdot\}$ represents the statistical expectation, and $\arg(\cdot)$ stands for the argument of a complex number.

2. Signal model

Consider K narrowband sources impinging on a symmetric ULA of $2M+1$ sensors with inter-element spacing d, as shown in Fig. 1. Suppose the center of array be the phase reference point, the sig-

☆ Fully documented templates are available in the elsarticle package on CTAN.
* Corresponding author.
E-mail addresses: zz@uestc.edu.cn (Z. Zheng), 201621010411@std.uestc.edu.cn (M. Fu), wqwang@uestc.edu.cn (W.-Q. Wang), hcso@ee.cityu.edu.hk (H.C. So).

https://doi.org/10.1016/j.sigpro.2018.03.020
0165-1684/© 2018 Elsevier B.V. All rights reserved.

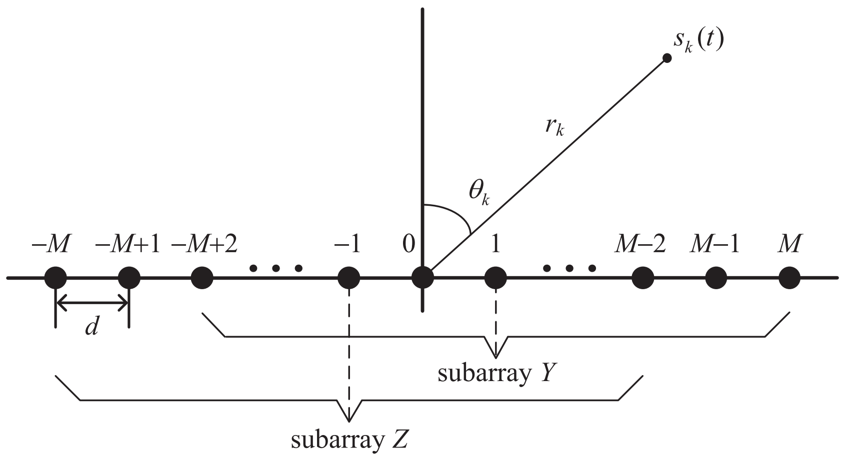

Fig. 1. Uniform linear array configuration.

nal received by the mth sensor can be expressed as [21,22]

$$x_m(t) = \sum_{k=1}^{K} s_k(t)e^{j\tau_{mk}} + n_m(t) \tag{1}$$

where $s_k(t)$ is the kth source waveform, $n_m(t)$ denotes the mth sensor noise, and τ_{mk} represents the propagation time of the kth source between the 0th and mth sensor. When the kth source is a near-field one, τ_{mk} has the following form:

$$\tau_{mk} = m\omega_k + m^2\phi_k \tag{2}$$

where ω_k and ϕ_k are given by

$$\omega_k = -2\pi\frac{d}{\lambda}\sin\theta_k \tag{3}$$

$$\phi_k = \pi\frac{d^2}{\lambda r_k}\cos^2\theta_k \tag{4}$$

with λ being the signal wavelength. θ_k and r_k are the DOA and range of the kth source, respectively. According to the definition of the Fresnel region [14], r_k should belong to the Fresnel region, i.e., $r_k \in [0.62(D^3/\lambda)^{1/2},\ 2D^2/\lambda]$, where $D = 2Md$ denotes the array aperture. Otherwise, if the kth source is a far-field one, τ_{mk} has the form of:

$$\tau_{mk} = m\omega_k. \tag{5}$$

In matrix form, (1) can be expressed as

$$\mathbf{x}(t) = \mathbf{A}_F\mathbf{s}_F(t) + \mathbf{A}_N\mathbf{s}_N(t) + \mathbf{n}(t) \tag{6}$$

where $\mathbf{y}(t)$ and $\mathbf{n}(t)$ are $(2M+1)\times 1$ complex vectors, and

$$\mathbf{x}(t) = [x_{-M}(t), \ldots, x_0(t), \ldots, x_M(t)]^T \tag{7}$$

$$\mathbf{A}_F = [\mathbf{a}(\theta_1), \ldots, \mathbf{a}(\theta_{K_1})] \tag{8}$$

$$\mathbf{A}_N = [\mathbf{a}(\theta_{K_1+1}, r_{K_1+1}), \ldots, \mathbf{a}(\theta_K, r_K)] \tag{9}$$

$$\mathbf{s}_F(t) = [s_1(t), \ldots, s_{K_1}(t)]^T \tag{10}$$

$$\mathbf{s}_N(t) = [s_{K_1+1}(t), \ldots, s_K(t)]^T \tag{11}$$

$$\mathbf{n}(t) = [n_{-M}(t), \ldots, n_0(t), \ldots, n_M(t)]^T \tag{12}$$

where

$$\mathbf{a}(\theta_k, r_k) = [e^{j(-M\omega_k+M^2\phi_k)}, \ldots, 1, \ldots, e^{j(M\omega_k+M^2\phi_k)}]^T \tag{13}$$

denotes the $(2M+1)\times 1$ steering vector. Note that in the received signal model (6), the first K_1 sources are assumed to be FF sources and the remaining $(K-K_1)$ are NF sources.

Throughout this paper, the following assumptions are required to hold:

(1) The source signals are statistically independent, zero-mean random processes with nonzero kurtosis.
(2) The sensor noise is additive spatially white Gaussian process with zero-mean, and independent of the source signals.
(3) The source number K is known or accurately estimated by the information theoretic criteria [32].

3. Proposed approach

3.1. DOA estimation of near-field and far-field sources

Based on the above assumptions, the fourth-order cumulant of the array outputs is defined as

$$\begin{aligned}
&\mathrm{cum}\{x_m(t), x_p^*(t), x_n^*(t), x_q(t)\} \\
&= \mathrm{cum}\left\{\sum_{k=1}^{K} s_k(t)e^{j(m\omega_k+m^2\phi_k)}, \left(\sum_{k=1}^{K} s_k(t)e^{j(p\omega_k+p^2\phi_k)}\right)^*, \right. \\
&\quad \left. \left(\sum_{k=1}^{K} s_k(t)e^{j(n\omega_k+n^2\phi_k)}\right)^*, \sum_{k=1}^{K} s_k(t)e^{j(q\omega_k+q^2\phi_k)}\right\} \\
&= \sum_{k=1}^{K} e^{j\{[(m-p)-(n-q)]\omega_k+[(m^2-p^2)-(n^2-q^2)]\phi_k\}} \\
&\quad \times \mathrm{cum}\{s_k(t), s_k^*(t), s_k^*(t), s_k(t)\} \\
&= \sum_{k=1}^{K} c_{4,s_k} e^{j\{[(m-p)-(n-q)]\omega_k+[(m^2-p^2)-(n^2-q^2)]\phi_k\}}
\end{aligned} \tag{14}$$

where $c_{4,s_k} = \mathrm{cum}\{s_k(t), s_k^*(t), s_k^*(t), s_k(t)\}$ is the kurtosis of the kth source signal, and $m, p, n, q \in [-M, M]$.

Let $p = -m$ and $q = -n$, (14) can be further written as

$$\begin{aligned}
&\mathrm{cum}\{x_m(t), x_{-m}^*(t), x_n^*(t), x_{-n}(t)\} \\
&= \sum_{k=1}^{K} c_{4,s_k} e^{j2m\omega_k}(e^{j2n\omega_k})^*, \quad m, n \in [-M, M].
\end{aligned} \tag{15}$$

As shown in Fig. 1, we divide the ULA into two overlapping subarrays Y and Z to construct two cross-cumulant matrices of the subarray outputs, from which we can derive the shift invariance structure in the cumulant domain. The received vectors of subarrays Y and Z are given by

$$\begin{aligned}\mathbf{y}(t) &= [y_{-M+1}(t), \ldots, y_0(t), \ldots, y_{M-1}(t)]^T \\ &= [x_{-M+2}(t), \ldots, x_1(t), \ldots, x_M(t)]^T,\end{aligned} \tag{16}$$

$$\begin{aligned}\mathbf{z}(t) &= [z_{-M+1}(t), \ldots, z_0(t), \ldots, z_{M-1}(t)]^T \\ &= [x_{-M}(t), \ldots, x_{-1}(t), \ldots, x_{M-2}(t)]^T.\end{aligned} \tag{17}$$

It is obvious that the mth element of $\mathbf{y}(t)$ is $x_{m+1}(t)$, while the mth element of $\mathbf{z}(t)$ is $x_{m-1}(t)$.

Using the subarray outputs and (15), we construct two cross-cumulant matrices $\mathbf{C}_1$ and $\mathbf{C}_2$. The $(\bar{m}, \bar{n})$th element of $\mathbf{C}_1$ and $\mathbf{C}_2$ are:

$$\begin{aligned}\mathbf{C}_1(\bar{m}, \bar{n}) &= \mathrm{cum}\{y_{\bar{m}-M}, z^*_{-(\bar{m}-M)}, y^*_{\bar{n}-M}, z_{-(\bar{n}-M)}\} \\ &= \mathrm{cum}\{x_{\bar{m}-M+1}, x^*_{-(\bar{m}-M+1)}, x^*_{\bar{n}-M+1}, \\ &\quad x_{-(\bar{n}-M+1)}\} \\ &= \sum_{k=1}^{K} c_{4,s_k} e^{j2(\bar{m}-M+1)\omega_k} (e^{j2(\bar{n}-M+1)\omega_k})^* \\ &= \sum_{k=1}^{K} c_{4,s_k} e^{j2(\bar{m}-M)\omega_k} (e^{j2(\bar{n}-M)\omega_k})^*\end{aligned} \tag{18}$$

$$\begin{aligned}\mathbf{C}_2(\bar{m}, \bar{n}) &= \mathrm{cum}\{y_{\bar{m}-M}, z^*_{-(\bar{m}-M)}, z^*_{\bar{n}-M}, y_{-(\bar{n}-M)}\} \\ &= \mathrm{cum}\{x_{\bar{m}-M+1}, x^*_{-(\bar{m}-M+1)}, x^*_{\bar{n}-M-1}, \\ &\quad x_{-(\bar{n}-M-1)}\} \\ &= \sum_{k=1}^{K} c_{4,s_k} e^{j2(\bar{m}-M+1)\omega_k} (e^{j2(\bar{n}-M-1)\omega_k})^* \\ &= \sum_{k=1}^{K} c_{4,s_k} e^{j2(\bar{m}-M)\omega_k} (e^{j2(\bar{n}-M)\omega_k})^* e^{j4\omega_k}\end{aligned} \tag{19}$$

where $\bar{m}, \bar{n} \in [1, 2M-1]$. Note that the cross-cumulant matrices $\mathbf{C}_1$ and $\mathbf{C}_2$ are only characterized by the DOAs.

In a compact matrix form, $\mathbf{C}_1$ is expressed as

$$\mathbf{C}_1 = \mathbf{B}\mathbf{C}_{4s}\mathbf{B}^H \tag{20}$$

where $\mathbf{C}_{4s} = \mathrm{diag}[c_{4,s_1}, c_{4,s_2}, \ldots, c_{4,s_K}]$, virtual "array manifold matrix" $\mathbf{B} = [\mathbf{b}(\theta_1), \ldots, \mathbf{b}(\theta_K)] \in \mathbb{C}^{(2M-1)\times K}$, and

$$\begin{aligned}\mathbf{b}(\theta_k) = [&e^{-j2(M-1)\omega_k}, e^{-j2(M-2)\omega_k}, \ldots, 1, \ldots, \\ &e^{j2(M-2)\omega_k}, e^{j2(M-1)\omega_k}]^T.\end{aligned} \tag{21}$$

Similarly, $\mathbf{C}_2$ can also be represented as

$$\mathbf{C}_2 = \mathbf{B}\boldsymbol{\Phi}\mathbf{C}_{4s}\mathbf{B}^H \tag{22}$$

where $\boldsymbol{\Phi} = \mathrm{diag}[e^{j4\omega_1}, e^{j4\omega_2}, \ldots, e^{j4\omega_K}]$.

Combining $\mathbf{C}_1$ and $\mathbf{C}_2$, we form the $(4M-2)\times(4M-2)$ matrix:

$$\mathbf{C} = \begin{bmatrix} \mathbf{C}_1 & \mathbf{C}_2^H \\ \mathbf{C}_2 & \mathbf{C}_1 \end{bmatrix} = \bar{\mathbf{B}}\mathbf{C}_{4s}\bar{\mathbf{B}}^H \tag{23}$$

where

$$\bar{\mathbf{B}} = \begin{bmatrix} \mathbf{B} \\ \mathbf{B}\boldsymbol{\Phi} \end{bmatrix} \in \mathbb{C}^{(4M-2)\times K}. \tag{24}$$

Performing eigenvalue decomposition (EVD) of $\mathbf{C}$ yields

$$\mathbf{C} = \mathbf{E}_s\boldsymbol{\Lambda}_s\mathbf{E}_s^H + \mathbf{E}_n\boldsymbol{\Lambda}_n\mathbf{E}_n^H \tag{25}$$

where $\boldsymbol{\Lambda}_s \in \mathbb{C}^{K\times K}$ and $\boldsymbol{\Lambda}_n \in \mathbb{C}^{(4M-2-K)\times(4M-2-K)}$ are the diagonal matrices containing the K largest and $(4M-2-K)$ smallest eigenvalues of $\mathbf{C}$, respectively, $\mathbf{E}_s \in \mathbb{C}^{(4M-2)\times K}$ and $\mathbf{E}_n \in \mathbb{C}^{(4M-2)\times(4M-2-K)}$ are composed of the eigenvectors of $\mathbf{C}$ corresponding to the K largest and $(4M-2-K)$ smallest eigenvalues, respectively.

Based on the subspace theory, $\mathbf{E}_s$ spans the column space of $\bar{\mathbf{B}}$. This means that there is an invertible $K\times K$ matrix $\mathbf{T}$ such that

$$\mathbf{E}_s = \bar{\mathbf{B}}\mathbf{T}. \tag{26}$$

Let $\mathbf{E}_1$ and $\mathbf{E}_2$ be the upper and the lower $(2M-1)\times K$ half matrices of $\mathbf{E}_s$, respectively. From (26), we have

$$\mathbf{E}_1 = \mathbf{B}\mathbf{T}, \ \mathbf{E}_2 = \mathbf{B}\boldsymbol{\Phi}\mathbf{T} \tag{27}$$

The relations in (27) is combined to result in

$$\mathbf{E}_2 = \mathbf{E}_1\boldsymbol{\Psi} \tag{28}$$

where $\boldsymbol{\Psi} = \mathbf{T}^{-1}\boldsymbol{\Phi}\mathbf{T}$. Eq. (28) can be solved by the TLS criterion [6] to find $\boldsymbol{\Psi}$ whose eigenvalues are related to the DOAs of sources. Let $\mathbf{V}$ be the $2K\times 2K$ matrix of right singular vectors of the matrix $[\hat{\mathbf{E}}_1 \ \hat{\mathbf{E}}_2]$. If the matrix is partitioned into four $K\times K$ submatrices as

$$\mathbf{V} = \begin{bmatrix} \mathbf{V}_{11} & \mathbf{V}_{12} \\ \mathbf{V}_{21} & \mathbf{V}_{22} \end{bmatrix}, \tag{29}$$

then the solution of (28) is given by

$$\hat{\boldsymbol{\Psi}} = -\mathbf{V}_{12}\mathbf{V}_{22}^{-1}. \tag{30}$$

Assuming that γ_k is the kth eigenvalue of $\hat{\boldsymbol{\Psi}}$, the DOA estimate of the kth source is

$$\hat{\theta}_k = \sin^{-1}\left(-\frac{\arg(\gamma_k)}{8\pi d/\lambda}\right), \quad k = 1, \cdots, K \tag{31}$$

3.2. Source classification and range estimation

Now we perform EVD on the covariance matrix $\mathbf{R} = E\{\mathbf{x}(t)\mathbf{x}^H(t)\}$:

$$\mathbf{R} = \mathbf{U}_s\boldsymbol{\Sigma}_s\mathbf{U}_s^H + \mathbf{U}_n\boldsymbol{\Sigma}_n\mathbf{U}_n^H \tag{32}$$

where $\boldsymbol{\Sigma}_s \in \mathbb{C}^{K\times K}$ and $\boldsymbol{\Sigma}_n \in \mathbb{C}^{(2M+1-K)\times(2M+1-K)}$ are the diagonal matrices containing the K largest and $(2M+1-K)$ smallest eigenvalues of $\mathbf{R}$, respectively, $\mathbf{U}_s \in \mathbb{C}^{(2M+1)\times K}$ and $\mathbf{U}_n \in \mathbb{C}^{(2M+1)\times(2M+1-K)}$ are composed of the eigenvectors of $\mathbf{R}$ corresponding to the K largest and $(2M+1-K)$ smallest eigenvalues, respectively.

With the DOA estimates $\{\hat{\theta}_k, \ k = 1, \ldots, K\}$, the range estimates $\{\hat{r}_k, \ k = 1, \ldots, K\}$ are obtained by substituting each $\hat{\theta}_k$ into the following spectral function

$$f(\theta, r) = \left[\mathbf{a}^H(\theta, r)\mathbf{U}_n\mathbf{U}_n^H\mathbf{a}(\theta, r)\right]^{-1}. \tag{33}$$

Note that $\hat{\theta}_k$ and $\hat{r}_k$ achieve automatic pairing without any extra processing. In fact, we can easily distinguish the types of sources. When $\hat{r}_k \in [0.62(D^3/\lambda)^{1/2}, 2D^2/\lambda]$, the kth source is a near-field one. On the contrary, when $\hat{r}_k \in [2D^2/\lambda, +\infty)$, the kth source is a far-field one and let $\hat{r}_k$ be ∞.

3.3. Discussion

1) Element Spacing Requirement: It is worth noting that the proposed algorithm requires $d \le \lambda/8$ to avoid the ambiguity of the phase for the elements of $\boldsymbol{\Phi}$, $e^{j4\omega_k} = e^{-j8\pi d/\lambda \sin\theta_k}$, $k = 1, \ldots, K$. *2) Source Number Limitation:* Since the dimension of fourth-order cumulant matrix $\mathbf{C}_1$ and $\mathbf{C}_2$ is $2M-1$, the proposed algorithm can locate $2M-2$ sources at most using a ULA of $2M+1$ sensors. In contrast, second-order MUSIC and high-order MUSIC

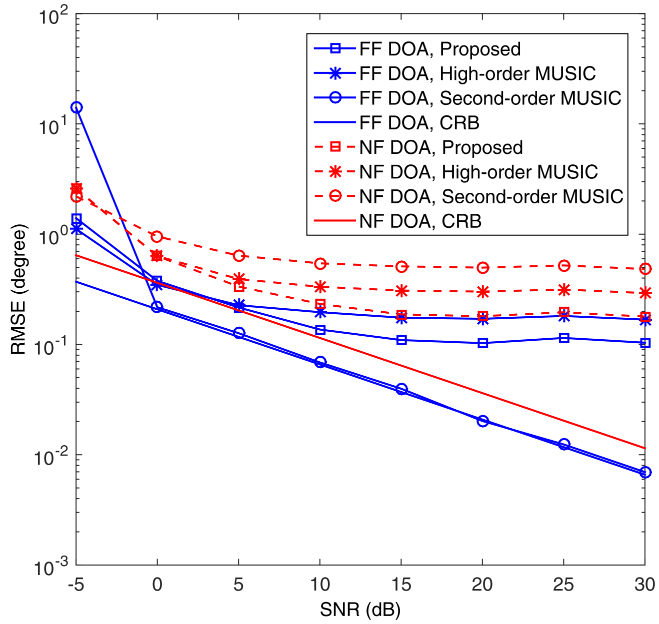

Fig. 2. RMSEs of DOA estimates for one FF and one NF source versus SNR.

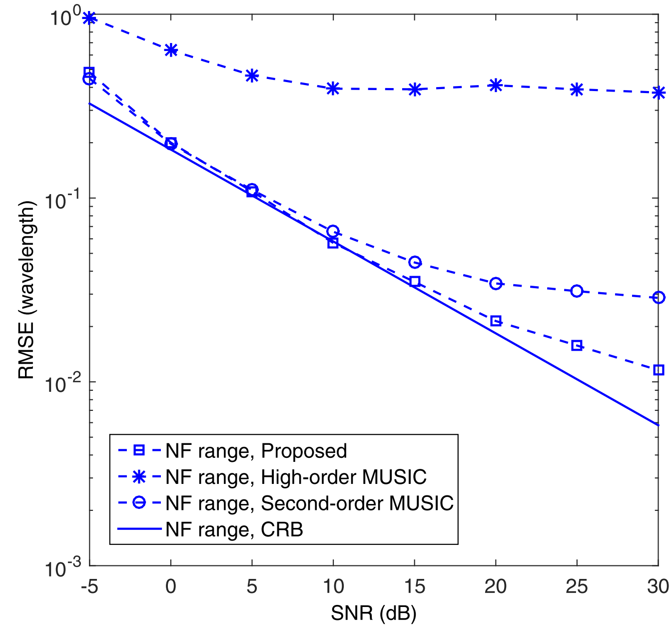

Fig. 3. RMSEs of range estimates for one FF and one NF source versus SNR.

can deal with up to M and $2M$ sources, respectively [21,22]. *3) Computational Complexity:* For the proposed algorithm, the major computations involve cumulant matrix construction, covariance matrix construction, their EVDs and range search, the resulting multiplications required are $O(18(2M-1)^2N + \frac{4}{3}(4M-2)^3 + (2M+1)^2N + \frac{4}{3}(2M+1)^3 + KS_r(2M+1)^2)$, where S_r is the number of search points in the Fresnel region. While high-order MUSIC and second-order MUSIC need to perform DOA search besides range search, and their multiplications are respectively $O(9(2M+1)^2N + 9(4M+1)^2N + \frac{4}{3}(2M+1)^3 + \frac{4}{3}(4M+1)^3 + \frac{4}{3}(2M+1)^2K + S_\theta(2M+1)^2)$ and $O((2M+1)^2N + (M+2)^2N + \frac{4}{3}(2M+1)^3 + \frac{4}{3}(M+2)^3 + 2S_\theta(2M+1)^2 + (K-K_1)S_r(2M+1)^2)$, where S_θ is the number of search points in the angular domain. Note that the proposed approach does not include $O(S_\theta(2M+1)^2)$, while both second-order MUSIC and high-order MUSIC contain a complexity of $O(S_\theta(2M+1)^2)$. Obviously, the proposed approach has lower computational burden than high-order MUSIC.

4. Simulation results

In this section, simulation examples are presented to assess the proposed algorithm, which is compared to the high-order MUSIC [21], second-order MUSIC [22] and Cramer–Rao bound (CRB) [22]. A 11-element ULA with inter-element spacing $d = \lambda/8$ is considered, and its Fresnel region is $0.8665\lambda < r < 3.125\lambda$. The additive noise is assumed to be spatial white complex Gaussian, and the signal-to-noise ratio (SNR) is defined relative to each signal. The results are evaluated by the root mean square error (RMSE) based on 500 Monte-Carlo trials.

In the first example, we consider the mixed source scenario with one far-field source and one near-field source, which are located at $(-5^\circ, +\infty)$ and $(55^\circ, 1.5\lambda)$, respectively. The SNR varies from −5 dB to 30 dB, and the number of snapshots is set as $N = 600$. Figs. 2 and 3 respectively display the RMSEs of DOA and range estimates using the proposed algorithm. For comparison, the RMSEs of high-order MUSIC, second-order MUSIC and the CRB are also presented. As it can be seen, second-order MUSIC has the best performance for FF DOA estimation, which is close to the CRB across a wide range of SNR, but it suffers severe performance degradation when the SNR is less than 0 dB. In contrast, the proposed method and high-order MUSIC achieve better performance at low SNRs because the cumulants can restrain the noise effect. For NF DOA estimation, the proposed method outperforms both second-order MUSIC and high-order MUSIC. Jointly considering FF and NF DOA estimation, the proposed method is also better than the latter two, as shown in Fig. 4. For NF range estimation, the proposed method has obvious advantages over high-order MUSIC, and it also outperforms second-order MUSIC at high SNRs.

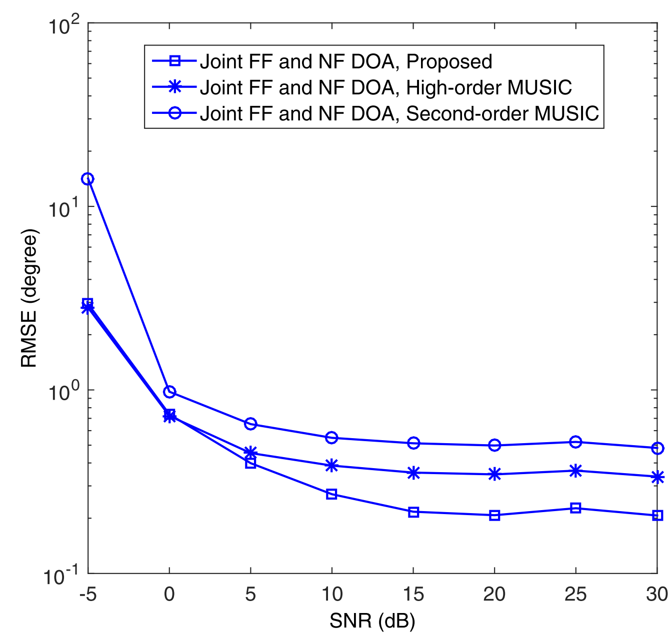

Fig. 4. RMSEs of joint FF and NF DOA estimates for one FF and one NF source versus SNR.

In the second example, we consider the situation with only two near-field sources. The other simulation parameters are the same with those in the first example, except that two near-field sources are located at $(-5^\circ, 1.45\lambda)$ and $(50^\circ, 1.6\lambda)$. The RMSEs of DOA and range estimates using the proposed algorithm are respectively shown in Figs. 5 and 6, where the RMSEs of high-order MUSIC,

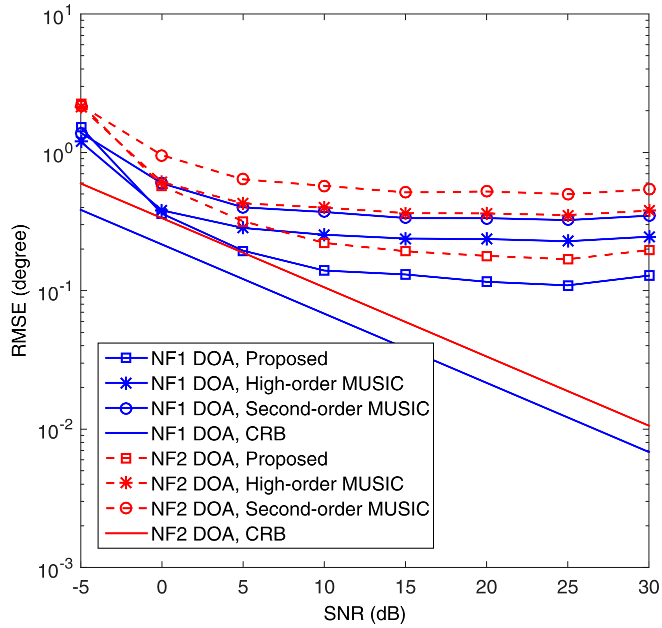

Fig. 5. RMSEs of DOA estimates for two NF sources versus SNR.

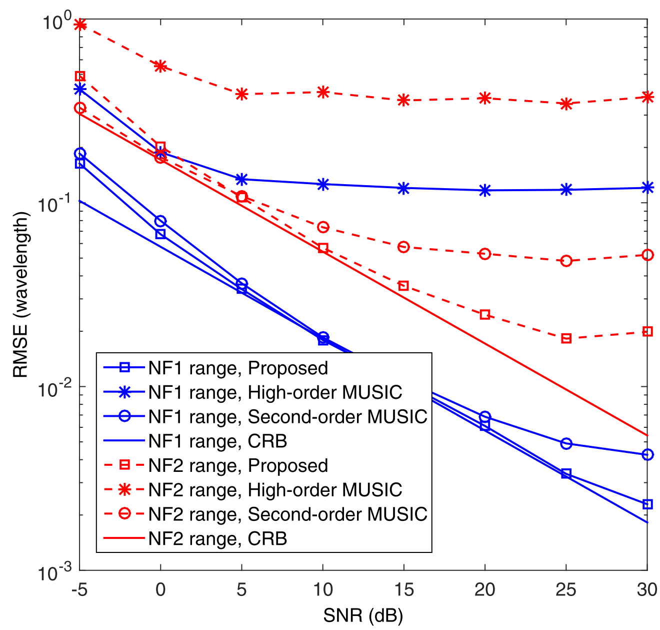

Fig. 6. RMSEs of range estimates for two NF sources versus SNR.

second-order MUSIC and the CRB are also plotted for comparison. For two NF sources, the proposed method exhibits better DOA estimates than both high-order MUSIC and second-order MUSIC across a wide range of SNR. For NF range estimation, both the proposed method and second-order MUSIC are obviously better than high-order MUSIC, but the proposed method outperforms second-order MUSIC at high SNRs. Therefore, our approach has higher localization accuracy than Liang and Liu [21] and He et al. [22] in near-field source scenarios.

5. Conclusion

In this paper, a new approach for mixed source localization has been developed. The presented approach performs DOA estimation based on the shift invariance structure in the cumulant domain, and estimates the ranges of sources by 1-D search. Compared to the existing methods, our approach does not require DOA search and parameter pairing, and thus it is computationally more efficient. Simulation results indicate that the presented approach achieves better performance than traditional methods including the second-order MUSIC and high-order MUSIC in near-field and mixed source scenarios.

Acknowledgment

This work is supported in part by the National Natural Science Foundation of China under Grants 61301155, 61571081 and 61703076, the 111 project (B14039), and the Fundamental Research Funds for the Central Universities of China under Grant ZYGX2016J008.

References

[1] H. Krim, M. Viberg, Two decades of array signal processing research: the parametric approach, IEEE Signal Process. Mag. 13 (4) (1996) 67–94.
[2] M.N.E. Korso, R. Boyer, A. Renaux, S. Marcos, Conditional and unconditional cramér–rao bounds for near-field source localization, IEEE Trans. Signal Process. 58 (5) (2010) 2901–2907.
[3] M.N.E. Korso, R. Boyer, A. Renaux, S. Marcos, Statistical analysis of achievable resolution limit in the near field source localization context, Signal Process. 92 (2) (2012) 547–552.
[4] J.P. Delmas, M.N.E. Korso, H. Gazzah, M. Castella, CRB analysis of planar antenna arrays for optimizing near-field source localization, Signal Process. 127 (2016) 117–134.
[5] R. Schmidt, Multiple emitter location and signal parameter estimation, IEEE Trans. Antennas Propag. 34 (3) (1986) 276–280.
[6] R. Roy, T. Kailath, ESPRIT-estimation of signal parameters via rotational invariance techniques, IEEE Trans. Acoust. Speech Signal Process. 37 (7) (1989) 984–995.
[7] Y.D. Huang, M. Barkat, Near-field multiple source localization by passive sensor array, IEEE Trans. Antennas Propag. 39 (7) (1991) 968–975.
[8] A. Weiss, B. Friedlander, Range and bearing estimation using polynomial rooting, IEEE J. Ocean. Eng. 18 (2) (1993) 130–137.
[9] D. Starer, A. Nehorai, Passive localization of near-field sources by path following, IEEE Trans. Signal Process. 42 (3) (1994) 677–680.
[10] J.H. Lee, Y.M. Chen, C.C. Yeh, A covariance approximation method for near-field direction-finding using a uniform linear array, IEEE Trans. Signal Process. 43 (5) (1995) 1293–1298.
[11] R.N. Challa, S. Shamsunder, High-order subspace-based algorithms for passive localization of near-field sources, in: Proc. 29th Asilomar Conf. Signals, Syst., Comput., 2, Pacific Grove, CA, 1995, pp. 777–781.
[12] E. Grosicki, K. Abed-Meraim, Y. Hua, A weighted linear prediction method for near-field source localization, IEEE Trans. Signal Process. 53 (10) (2005) 3651–3660.
[13] Y. Wu, L. Ma, C. Hou, G. Zhang, J. Li, Subspace-based method for joint range and DOA estimation of multiple near-field sources, Signal Process. 86 (8) (2006) 2129–2133.
[14] W. Zhi, M.Y.W. Chia, Near-field source localization via symmetric subarrays, IEEE Signal Process. Lett. 14 (6) (2007) 409–412.
[15] W.J. Zeng, X.L. Li, H. Zou, X.D. Zhang, Near-field multiple source localization using joint diagonalization, Signal Process. 89 (2) (2009) 232–238.
[16] J. Liang, X. Zeng, B. Ji, J. Zhang, F. Zhao, A computationally efficient algorithm for joint range–DOA–frequency estimation of near-field sources, Digital Signal Process. 19 (4) (2009) 596–611.
[17] J. Liang, D. Liu, Passive localization of near-field sources using cumulant, IEEE Sensors J. 9 (8) (2009) 953–960.
[18] J.A. Chaaya, J. Picheral, S. Marcos, Localization of spatially distributed near–field sources with unknown angular spread shape, Signal Process. 106 (2015) 259–265.
[19] J. Xie, H. Tao, X. Rao, J. Su, Efficient method of passive localization for near-field noncircular sources, IEEE Antennas Wireless Propag. Lett. 14 (2015) 1223–1226.
[20] L. Jianzhong, Y. Wang, W. Gang, Signal reconstruction for near-field source localisation, IET Signal Process. 9 (3) (2015) 201–205.
[21] J. Liang, D. Liu, Passive localization of mixed near-field and far-field sources using two-stage MUSIC algorithm, IEEE Trans. Signal Process. 58 (1) (2010) 108–120.
[22] J. He, M. Swamy, M.O. Ahmad, Efficient application of MUSIC algorithm under the coexistence of far-field and near-field sources, IEEE Trans. Signal Process. 60 (4) (2012) 2066–2070.
[23] B. Wang, Y. Zhao, J. Liu, Mixed-order MUSIC algorithm for localization of far–field and near-field sources, IEEE Signal Process. Lett. 20 (4) (2013) 311–314.
[24] B. Wang, J. Liu, X. Sun, Mixed sources localization based on sparse signal reconstruction, IEEE Signal Process. Lett. 19 (8) (2012) 487–490.
[25] Y. Tian, X. Sun, Mixed sources localisation using a sparse representation of cumulant vectors, IET Signal Process. 8 (6) (2014) 606–611.

[26] G. Liu, X. Sun, Two-stage matrix differencing algorithm for mixed far-field and near-field sources classification and localization, IEEE Sensors J. 14 (6) (2014) 1957–1965.
[27] G. Liu, X. Sun, Spatial differencing method for mixed far-field and near-field sources localization, IEEE Signal Process. Lett. 21 (11) (2014) 1331–1335.
[28] G. Liu, X. Sun, Efficient method of passive localization for mixed far-field and near-field sources, IEEE Antennas Wireless Propag. Lett. 12 (2013) 902–905.
[29] G. Liu, X. Sun, Y. Liu, Y. Qin, Low-complexity estimation of signal parameters via rotational invariance techniques algorithm for mixed far-field and near-field cyclostationary sources localisation, IET Signal Process. 7 (5) (2013) 382–388.
[30] J. Jiang, F. Duan, J. Chen, Y. Li, X. Hua, Mixed near-field and far-field sources localization using the uniform linear sensor array, IEEE Sensors J. 13 (8) (2013) 3136–3143.
[31] F. Gao, A.B. Gershman, A generalized ESPRIT approach to direction-of-arrival estimation, IEEE Signal Process. Lett. 12 (3) (2005) 254–257.
[32] M. Wax, T. Kailath, Detection of signals by information theoretic criteria, IEEE Trans. Acoust. Speech Signal Process. ASSP-33 (2) (1985) 387–392.